Xu, Y., Caijin, Y., Zhang, W., Zhu, W., and Fan, W. (January 7, 2022). "A New Moving Kirchhoff-Love Plate Element for Dynamic Analysis of Vehicle-Pavement Interaction." ASME. J. Vib. Acoust.
doi: https://doi.org/10.1115/1.4053474

Journal of Vibration and Acoustics. Received August 20, 2021;
Accepted manuscript posted December 27, 2021. doi:10.1115/1.4053474

A New Moving Kirchhoff-Love Plate Element for Dynamic Analysis of Vehicle-Pavement Interaction

Xu Yan

State Key Laboratory of Traction Power, Southwest Jiaotong University, Chengdu, 610031 China

Email: 1533594664@qq.com

Yang Caijing*

State Key Laboratory of Traction Power, Southwest Jiaotong University, Chengdu, 610031 China

Email: ycj78_2012@163.com

Zhang Weihua

State Key Laboratory of Traction Power, Southwest Jiaotong University, Chengdu, 610031 China

Email: tpl@swjtu.edu.cn

Zhu Weidong

Department of Mechanical Engineering, University of Maryland, Baltimore County, Baltimore, MD 21250, USA

Email: wzhu@umbc.edu

Fan Wei

Department of Academy of Astronautics, Harbin Institute of Technology, Harbin, 150001, China

Email: fanweiscu@scu.edu.cn

* Corresponding author

Journal of Vibration and Acoustics. Received August 20, 2021;
Accepted manuscript posted December 27, 2021. doi:10.1115/1.4053474

Abstract: A new moving Kirchhoff-Love plate element is developed in this work to accurately and efficiently calculate the dynamic response of vehicle-pavement interaction. Since the vehicle can only affect a small region nearby, the wide pavement is reduced to a small reduced plate area around the vehicle. The vehicle loads moving along an arbitrary trajectory is considered, and the arbitrary Lagrangian-Eulerian method is used here for coordinate conversion. The reduced plate area is spatially discretized using the current moving plate element, where its governing equations are derived using Lagrange's equations. The moving plate element is validated by different plate subjected to moving load cases, where the influences of different factors on reduced plate area length of the RBM model are also investigated. Then a vehicle-pavement interaction case with constant and variable speed is analyzed here. The calculation results from the moving plate element are in good agreement with those from the modal superposition method (MSM), and the calculation time with the moving plate element is only one third of that using the MSM. It is also found that the moving load velocity and ground damping have great influences on reduced plate area length of the RBM. The moving plate element is accurate and more efficient than the MSM in calculating the dynamic response of the vehicle-pavement interaction.

Keywords: Moving Kirchhoff-Love plate element, arbitrary Lagrangian-Eulerian method, arbitrary moving load trajectory, vehicle-pavement interaction.

1. Introduction

The vehicle-pavement interaction plays an important role both in vehicle engineering [1]

and road engineering [2]. With the increasing of road traffic and vehicle loads, the road damage caused by the vehicle-pavement interaction occurs more frequently, which has caused the poor condition of the road and the decreasing of its serviceability [3]. The poor condition of the road also obviously influences the ride comfort of passengers and running safety of vehicles [4]. The road damage has greatly increased the cost of maintenance on the road. For example, the US Federal Highway Administration (FHWA) spent 182 billion dollars on improvement and maintenance of the federal highway in 2008 [4]. To prevent the road damage and decrease the cost of maintenance of the road, the vehicle-pavement interaction should be carefully studied nowadays.

Many scholars have investigated the vehicle-pavement interaction problems from different aspects, including the dynamic characteristics of the rigid pavements [5], pavement life cycle assessment (LCA) [6], predicting tire contact stresses [7], etc.. When analyzing these problems, different methods are applied in the modeling of the vehicle-pavement interaction. Since the analytical method can only be used in those simple problems with no complex vehicle-pavement interaction forces included [8], the numerical method is mainly applied here, which mainly includes the modal superposition method (MSM) and finite element method (FEM). The MSM has been applied by many researchers to study the dynamic responses of the vehicle-pavement interaction in an engineering environment. Li et al. [9] developed a nonlinear vehicle–pavement interaction model to study the nonlinear dynamic responses of the pavement and vehicle in the vehicle–road interaction, where the MSM is used to model the pavement. Ding et al. [4] investigated the influence of different factors on dynamic responses of the vehicle-pavement interaction in two-dimensional. In their model, the pavement is considered

as Timoshenko beam and modeled through the MSM. The FEM is more widely used in modeling pavement structure in vehicle-pavement interaction cases. Behnke et al. [10] developed a vehicle-pavement model to predict the long-term dynamic responses of the pavement structure under different temperature, where the FEM is used and the time homogenization technique is combined with arbitrary Lagrangian Eulerian (ALE) method for modeling. Shi and Cai [11] modeled the three-dimensional (3D) vehicle–pavement interaction to study the influence of road surface conditions, vehicle parameters, and driving speed on the dynamic responses of the pavement. In their study, the pavement and foundation were modeled using the FEM. Qian et al. [12] investigated the random dynamic responses of the pavement in vehicle-pavement interaction, where the pavement is modeled as a layered finite element model established in commercial software ABAQUS.

It can be found from these published papers that vehicle-pavement interaction with limited pavement area have been comprehensively studied using the FEM and MSM. However, when studying those long-term related vehicle-pavement interaction problems like the formation mechanism of rutting and heavy truck tread wear, the vehicle moving on the pavement in the long term should be considered and modeled to analyze the long-term dynamic behavior of the pavement and vehicle. Therefore, the pavement used in the modeling needs to be of large scale, which results in a huge number of elements in the FEM model and modes in the MSM model. As a result, the calculation speed of the dynamic response of the vehicle-pavement interaction will obviously decrease. To solve these problems, the moving coordinate system [13] is developed at first, and then the moving element method (MEM) [14] based on the moving coordinate system are applied in these problems. In these two methods, the plate structure is

Journal of Vibration and Acoustics. Received August 20, 2021;
Accepted manuscript posted December 27, 2021. doi:10.1115/1.4053474

reduced to a small region around the moving vehicle with most of the beam vibrations included and the length of this region is assumed to be long enough to eliminate reflections at the boundaries. Since only a small region instead of the whole plate need to be modeled, the number of degrees of freedom (DOFs) of the vehicle-pavement interaction system is greatly reduced and its calculation efficiency is significantly increased. Many researchers have used these two methods in solving different vehicle-pavement interaction problems [15-17]. However, the moving coordinate system and MEM only considers the vehicle moving along a straight trajectory with constant speed, and some paper even simplifies the pavement into beam structure under this situation [17]. This has limit their application in complex vehicle-pavement interaction problems and other related plate structure subjected to moving loads cases, where the loads may moving along a non-straight trajectory.

A new Kirchhoff–Love theory-based four-nodes moving plate element (MPE) is developed here to calculate in an efficient and accurate way the dynamic response of vehicle-pavement interaction with an arbitrary trajectory. The reduced plate area around the moving load mentioned above is further included in a control volume [18] attached to the moving load, and the vibration of the plate dissipates at the boundaries of the control volume. After the formulation of the moving control volume, a relative coordinate system is considered attached to the moving control volume, and the MPE is formulated in this relative coordinate system. Because the material of the plate is at rest in the global coordinated system and moves in the relative coordinate system, the MPE is not a physical element like a traditional plate element. The relative motion between the plate material point and the MPE is first considered here and formulated based on the ALE formulation. The ALE formulation is used here to translate the

Journal of Vibration and Acoustics. Received August 20, 2021;
Accepted manuscript posted December 27, 2021. doi:10.1115/1.4053474

system of the MPE into the global coordinated system, and the Lagrange equation is applied to obtain the final dynamic equations of the MPE. Because only the small reduced plate area needs to be modeled, the efficiency of the MPE is remarkably increased compared to the traditional FEM and MSM in calculating the dynamic responses of a vehicle-pavement interaction. Moreover, because the ALE formulation is employed, the MPE can calculate the dynamic responses of the pavement under vehicle loads moving along an arbitrary trajectory and varying speed in a long term. In summary, compared to the existing plate element, the MPE is a valuable tool in the investigation of problems of vehicle-pavement interaction with arbitrary trajectories and taking into account the velocity. The MPE is very suitable for the analysis of the long-term dynamic behavior of vehicle–pavement interaction, and it can also be used in studying more general plate structure subjected to moving load problems.

To verify the accuracy of the MPE, a thin plate resting on Winkler foundation and subjected to a constant concentrate load moving along different trajectories is considered at first. The dynamic responses of the plate are calculated using the MPE and compared with those from the commercial software ANSYS and semi-analytical solution [19]. To further investigate the characteristics of the MPE, the influence of different factors on reduced plate area length of the RBM model is investigated here. The MPE is then used to solve the dynamic responses of the vehicle-pavement interaction with constant and variable vehicle moving speed. The corresponding results are also compared with those from the traditional model developed in Ref. [9], where the MSM is used in modeling. The calculation results show that the MPE is accurate and efficient in solving long-term vehicle-pavement interaction problems.

The remainder of this paper is organized as follows. The new MPE is developed in Section

2, and its basic numerical results are presented in Section 3. The applicability of the MPE to the dynamic analysis of vehicle–pavement interaction is further verified in Section 4, and its efficiency is illustrated in Section 5. Some meaningful conclusions are provided in Section 6.

2. Theoretical formulation of the moving plate element

2.1 Basic theory

A rectangular MPE with four nodes is considered in the reduced plate area around the moving load, as shown in Fig. 1. The nodes I_1, I_2, I_3, and I_4 are located on the middle surface of the MPE. Because the thickness of the plate structure is much smaller than its length and width (ratio smaller than 0.1) in many structures such as slabs and pavements, the Kirchhoff–Love theory is used here. Therefore, each node of the MPE has three degrees of freedom, which are the vertical translation w_I and the rotations of the plate cross-section around the *x* and *y* axes, θ_{xI} and θ_{yI}. Considering an arbitrary plate material point *P* on the plate, based on the ALE formulation [20], the relationship between the coordinates of the plate material points *x* and *y* in the reference coordinate *o-xyz* attached to the moving control volume and *X* and *Y* in the global coordinate system *O-XYZ* is as follows:

$$x = X - d_x(t), \quad y = Y - d_y(t) \tag{1}$$

where $d_x(t)$ and $d_y(t)$ are the distances between points *o* and *O* in the *x* and *y* directions, respectively. Differentiating Eq. (1) with time *t* yields

$$\dot{x} = -V_x(t), \quad \dot{y} = -V_y(t) \tag{2}$$

where $V_x(t)$ and $V_y(t)$ are the velocity functions of the moving load along the *x* and *y* directions, respectively.

Journal of Vibration and Acoustics. Received August 20, 2021;
Accepted manuscript posted December 27, 2021. doi:10.1115/1.4053474

The velocity vector of the arbitrary point *P* is further derived here based on the theory of 3D MBE and Kirchhoff-Love theory, which is

$$\begin{aligned}\mathbf{v}_P &= \dot{\mathbf{r}}_P = \left[\dot{u}(x,y,z,t), \dot{v}(x,y,z,t), \dot{w}(x,y,z,t)\right]^T \\ &= \left[\frac{\mathrm{d}}{\mathrm{d}t}\left(-z\frac{\partial w(x,y,t)}{\partial x}\right), \frac{\mathrm{d}}{\mathrm{d}t}\left(-z\frac{\partial w(x,y,t)}{\partial y}\right), \dot{w}(x,y,t)\right]^T\end{aligned} \tag{3}$$

where u, v, and w are the displacements of point *P* along the *x*, *y*, and *z* axes, respectively.

2.2 Kinematic and strain energy of the moving plate element

Based on Eq. (3), the kinematic energy of the MPE can be expressed as

$$\begin{aligned}T &= \frac{1}{2}\rho\int_\Omega \mathbf{v}_P^T\mathbf{v}_P d\Omega = \frac{1}{2}\rho\int_\Omega \left(z^2\dot{w}_x^2 + z^2\dot{w}_y^2 + \dot{w}^2\right)d\Omega \\ &= \frac{1}{2}\rho\int_\Omega z^2\left(\dot{w}_x^2 + \dot{w}_y^2\right)d\Omega + \frac{1}{2}\rho\int_\Omega\left(\dot{w}^2\right)d\Omega \\ &= \frac{1}{24}\rho h^3\iint_S\left(\dot{w}_x^2 + \dot{w}_y^2\right)dxdy + \frac{1}{2}\rho h\iint_S \dot{w}^2 dxdy\end{aligned} \tag{4}$$

where w_x and w_y denote the partial derivative of a variable with respect to *x*, *h* is the thickness of the MPE, *S* indicates the middle surface, and Ω indicates the volume of the plate element. Similarly, the strain energy of the MPE can be expressed as

$$U = \frac{1}{2}\iint_\Omega \boldsymbol{\kappa}^T\mathbf{D}\boldsymbol{\kappa}dxdy \tag{5}$$

where $\boldsymbol{\kappa}^T = \begin{bmatrix}\kappa_x & \kappa_y & \kappa_{xy}\end{bmatrix}$ is the generalized strain vector of the plate, $\mathbf{D}$ is the elasticity matrix, and

$$\kappa_x = -\frac{\partial^2 w}{\partial x^2},\ \kappa_y = -\frac{\partial^2 w}{\partial y^2},\ \kappa_{xy} = -2\frac{\partial^2 w}{\partial x\partial y} \tag{6}$$

$$\mathbf{D} = D_0\begin{bmatrix}1 & \nu & 0\\ \nu & 1 & 0\\ 0 & 0 & \dfrac{1-\nu}{2}\end{bmatrix} \tag{7}$$

In Eq. (7), D_0 is the plate rigidity, and ν is the Poisson's ratio.

Journal of Vibration and Acoustics. Received August 20, 2021;
Accepted manuscript posted December 27, 2021. doi:10.1115/1.4053474

2.3 Governing equations of the moving plate element

The governing equations of the MPE are derived as follows. Based on the finite element theory, the vertical displacement w can be expressed as

$$w = \mathbf{N}\mathbf{q} \tag{8}$$

where $\mathbf{N}$ is the standard shape function vector of the 4 nodes thin plate element, as shown in Ref. [5], and $\mathbf{q}$ is the generalized coordinate vector of the MPE. The expression of $\mathbf{q}$ is

$$\mathbf{q} = \left[\mathbf{q}_1, \mathbf{q}_2, \mathbf{q}_3, \mathbf{q}_4\right]^T \tag{9}$$

where

$$\mathbf{q}_i = \left[w_i, \frac{\partial w_i}{\partial y}, -\frac{\partial w_i}{\partial x} \right], i = 1, 2, 3, 4 \tag{10}$$

in which w_i is the vertical displacement of node *i*. Note that $\mathbf{N}$ is the function of *x* and *y* in *o-xyz*. Considering Eq. (8) in Eq. (4), one has

$$w_x = \frac{\partial \mathbf{N}}{\partial x}\mathbf{q} = \mathbf{N}_x\mathbf{q},\ w_y = \frac{\partial \mathbf{N}}{\partial y}\mathbf{q} = \mathbf{N}_y\mathbf{q} \tag{11}$$

and

$$\dot{w} = \left(-V_x(t)\mathbf{N}_x - V_y(t)\mathbf{N}_y\right)\mathbf{q} + \mathbf{N}\dot{\mathbf{q}},\quad \dot{w}_x = \left(-V_x(t)\mathbf{N}_{xx} - V_y(t)\mathbf{N}_{xy}\right)\mathbf{q} + \mathbf{N}_x\dot{\mathbf{q}} \tag{12}$$

$$\dot{w}_y = \left(-V_x(t)\mathbf{N}_{yx} - V_y(t)\mathbf{N}_{yy}\right)\mathbf{q} + \mathbf{N}_y\dot{\mathbf{q}} \tag{13}$$

Substituting Eqs. (12) and (13) in Eq. (4) yields

$$\begin{aligned} T &= \frac{1}{24}\rho h^3 \iint_S \left(\dot{w}_x^2 + \dot{w}_y^2\right) dxdy + \frac{1}{2}\rho h \iint_S \dot{w}^2 dxdy \\ &= \frac{1}{24}\rho h^3 \iint_S \begin{pmatrix} \left(\left(-V_x(t)\mathbf{N}_{xx} - V_y(t)\mathbf{N}_{xy}\right)\mathbf{q} + \mathbf{N}_x\dot{\mathbf{q}}\right)^2 \\ + \left(\left(-V_x(t)\mathbf{N}_{yx} - V_y(t)\mathbf{N}_{yy}\right)\mathbf{q} + \mathbf{N}_y\dot{\mathbf{q}}\right)^2 \end{pmatrix} dxdy \\ &+ \frac{1}{2}\rho h \iint_S \left(\left(-V_x(t)\mathbf{N}_x - V_y(t)\mathbf{N}_y\right)\mathbf{q} + \mathbf{N}\dot{\mathbf{q}}\right)^2 dxdy \end{aligned} \tag{14}$$

Considering Lagrange's equation, one can have

Journal of Vibration and Acoustics. Received August 20, 2021;
Accepted manuscript posted December 27, 2021. doi:10.1115/1.4053474

$$\frac{d}{dt}\left(\frac{\partial T}{\partial \dot{\mathbf{q}}}\right)-\frac{\partial T}{\partial \mathbf{q}}=\mathbf{M}\ddot{\mathbf{q}}+\mathbf{C}\dot{\mathbf{q}}+\mathbf{K}_0\mathbf{q}-\mathbf{Q}_{flow} \tag{15}$$

where

$$\begin{aligned}\mathbf{M}&=\frac{1}{12}\rho h^3\iint_S\left(\mathbf{N}_x^T\mathbf{N}_x+\mathbf{N}_y^T\mathbf{N}_y\right)dxdy\\&+\rho h\iint_S\left(\mathbf{N}^T\mathbf{N}\right)dxdy\end{aligned} \tag{16}$$

$$\begin{aligned}\mathbf{C}&=\frac{1}{12}\rho h^3\iint_S\begin{pmatrix}2\left(-V_x(t)\mathbf{N}_x^T\mathbf{N}_{xx}-V_y(t)\mathbf{N}_x^T\mathbf{N}_{xy}\right)\\+2\left(-V_x(t)\mathbf{N}_y^T\mathbf{N}_{yx}-V_y(t)\mathbf{N}_y^T\mathbf{N}_{yy}\right)\end{pmatrix}dxdy\\&+\rho h\iint_S\left(2\left(-V_x(t)\mathbf{N}^T\mathbf{N}_x-V_y(t)\mathbf{N}^T\mathbf{N}_y\right)\right)dxdy\end{aligned} \tag{17}$$

$$\begin{aligned}\mathbf{K}_0=\frac{1}{12}\rho h^3\iint_S&\left(\begin{pmatrix}-a_x(t)\mathbf{N}_x^T\mathbf{N}_{xx}+V_x^2(t)\mathbf{N}_x^T\mathbf{N}_{xxx}\\+V_x(t)V_y(t)\mathbf{N}_x^T\mathbf{N}_{xxy}-a_y(t)\mathbf{N}_x^T\mathbf{N}_{xy}\\+V_x(t)V_y(t)\mathbf{N}_x^T\mathbf{N}_{xyx}+V_y^2(t)\mathbf{N}_x^T\mathbf{N}_{xyy}\end{pmatrix}\right.\\&\left.+\begin{pmatrix}-a_x(t)\mathbf{N}_y^T\mathbf{N}_{yx}+V_x^2(t)\mathbf{N}_y^T\mathbf{N}_{yxx}\\+V_x(t)V_y(t)\mathbf{N}_y^T\mathbf{N}_{yxy}-a_y(t)\mathbf{N}_y^T\mathbf{N}_{yy}\\+V_x(t)V_y(t)\mathbf{N}_y^T\mathbf{N}_{yyx}+V_y^2(t)\mathbf{N}_y^T\mathbf{N}_{yyy}\end{pmatrix}\right)dxdy\\+\rho h\iint_S&\left(\begin{pmatrix}-a_x(t)\mathbf{N}^T\mathbf{N}_x+V_x^2(t)\mathbf{N}^T\mathbf{N}_{xx}+V_x(t)V_y(t)\mathbf{N}^T\mathbf{N}_{xy}\\-a_y(t)\mathbf{N}^T\mathbf{N}_y+V_x(t)V_y(t)\mathbf{N}^T\mathbf{N}_{yx}+V_y^2(t)\mathbf{N}^T\mathbf{N}_{yy}\end{pmatrix}\right)dxdy\end{aligned} \tag{18}$$

where $a_x(t)$ and $a_y(t)$ are the accelerations of the moving load along the x and y directions, respectively. In Eq. (18), there is

$$\mathbf{N}_{xxx}=\frac{\partial \mathbf{N}_{xx}}{\partial x}=\frac{\partial}{\partial x}\left(\frac{\partial \mathbf{N}_x}{\partial x}\right)=\frac{\partial}{\partial x}\left(\frac{\partial}{\partial x}\left(\frac{\partial \mathbf{N}}{\partial x}\right)\right) \tag{19}$$

and other similar terms can be derived through the same process. As mentioned before, because there is also a relative motion between the plate material and control volume, based on the familiar derivation progress shown in Ref. [16], the additional generalized force vector $\mathbf{Q}_{flow}$ also occurs here, which is

Journal of Vibration and Acoustics. Received August 20, 2021;
Accepted manuscript posted December 27, 2021. doi:10.1115/1.4053474

$$\begin{aligned}
\mathbf{Q}_{flow} = & V_x(t)\left.\begin{pmatrix} \frac{1}{12}\rho h^3\int_0^a\left(\left(-V_y(t)\mathbf{N}_y^T\mathbf{N}_{yy}\right)\mathbf{q}+\mathbf{N}_y^T\mathbf{N}_y\dot{\mathbf{q}}\right)dy \\ +\rho h\int_0^a\left(\left(-V_y(t)\mathbf{N}^T\mathbf{N}_y\right)\mathbf{q}+\mathbf{N}^T\mathbf{N}\dot{\mathbf{q}}\right)dy \end{pmatrix}\right|_{x=0} \\
& -V_x(t)\left.\begin{pmatrix} \frac{1}{12}\rho h^3\int_0^a\left(\left(-V_y(t)\mathbf{N}_y^T\mathbf{N}_{yy}\right)\mathbf{q}+\mathbf{N}_y^T\mathbf{N}_y\dot{\mathbf{q}}\right)dy \\ +\rho h\int_0^a\left(\left(-V_y(t)\mathbf{N}^T\mathbf{N}_y\right)\mathbf{q}+\mathbf{N}^T\mathbf{N}\dot{\mathbf{q}}\right)dy \end{pmatrix}\right|_{x=b} \\
& +V_y(t)\left.\begin{pmatrix} \frac{1}{12}\rho h^3\int_0^b\left(\left(-V_x(t)\mathbf{N}_x^T\mathbf{N}_{xx}\right)\mathbf{q}+\mathbf{N}_x^T\mathbf{N}_x\dot{\mathbf{q}}\right)dx \\ +\rho h\int_0^b\left(\left(-V_x(t)\mathbf{N}^T\mathbf{N}_x\right)\mathbf{q}+\mathbf{N}^T\mathbf{N}\dot{\mathbf{q}}\right)dx \end{pmatrix}\right|_{y=0} \\
& -V_y(t)\left.\begin{pmatrix} \frac{1}{12}\rho h^3\int_0^b\left(\left(-V_x(t)\mathbf{N}_x^T\mathbf{N}_{xx}\right)\mathbf{q}+\mathbf{N}_x^T\mathbf{N}_x\dot{\mathbf{q}}\right)dx \\ +\rho h\int_0^b\left(\left(-V_x(t)\mathbf{N}^T\mathbf{N}_x\right)\mathbf{q}+\mathbf{N}^T\mathbf{N}\dot{\mathbf{q}}\right)dx \end{pmatrix}\right|_{y=a}
\end{aligned} \tag{20}$$

where a and b are the length and width of the plate element, respectively. The detailed derivation can be found in Ref. [18]. Note that this additional generalized force vector $\mathbf{Q}_{flow}$ is close to zero.

Similarly, considering Eq. (8) into Eq. (5), one can obtain

$$\kappa_x = -\mathbf{N}_{xx}\mathbf{q},\ \ \kappa_y = -\mathbf{N}_{yy}\mathbf{q},\ \ \kappa_{xy} = -2\mathbf{N}_{xy}\mathbf{q} \tag{21}$$

and

$$\boldsymbol{\kappa} = \left[-\mathbf{N}_{xx}, -\mathbf{N}_{yy}, -2\mathbf{N}_{xy}\right]^T\mathbf{q} = \mathbf{N}_S\mathbf{q} \tag{22}$$

Substituting Eq. (21) into Eq. (5) yields

$$U = \frac{1}{2}\iint_\Omega \mathbf{q}^T\mathbf{N}_S^T\mathbf{D}\mathbf{N}_S\mathbf{q}dxdy \tag{23}$$

Based on the Lagrange's equation, there is

$$\frac{\partial U}{\partial \mathbf{q}} = \iint_\Omega \mathbf{N}_S^T\mathbf{D}\mathbf{N}_S dxdy\mathbf{q} \tag{24}$$

Consider an arbitrary external force **F** applied on the MPE at a point whose coordinate vector is $\left(x_F, y_F, z_F\right)^T$. The displacement vector of the load acting point can be expressed as

$$\begin{aligned}\mathbf{r}_F &= \left[-z\frac{\partial w(x_F,y_F,t)}{\partial x_F}, -z\frac{\partial w(x_F,y_F,t)}{\partial y_F}, w(x_F,y_F,t)\right]^T \\ &= \left[-z\mathbf{N}_{xF}, -z\mathbf{N}_{yF}, \mathbf{N}_F\right]^T \mathbf{q} = \mathbf{R}_F\mathbf{q}\end{aligned} \tag{25}$$

where $w(x_F, y_F, t)$ is the vertical displacement of the pavement at the load acting point, and $\mathbf{N}_F$ is the corresponding shape functions. The virtual work done by **F** is

$$\delta W_F = \delta \mathbf{r}_F^T \mathbf{F} = \delta \mathbf{q}^T \mathbf{Q} \tag{26}$$

and the generalized force vector $\mathbf{Q}$ is

$$\mathbf{Q} = \mathbf{R}_F^T \mathbf{F} \tag{27}$$

Based on Eqs. (15), (20), (24), and (27), one can obtain the governing equation of the MPE, which is

$$\mathbf{M}\ddot{\mathbf{q}} + \mathbf{C}\dot{\mathbf{q}} + \mathbf{K}\mathbf{q} = \mathbf{Q} + \mathbf{Q}_{flow} \tag{28}$$

where $\mathbf{K} = \mathbf{K}_0 + \mathbf{K}_1$, and

$$\mathbf{K}_1 = \iint_\Omega \mathbf{N}_S^T \mathbf{D} \mathbf{N}_S dxdy \tag{29}$$

Note that the position of the moving load in the *xoy* plane does not change with time.

Based on the dynamic equations of a single MPE, the dynamic equations of the whole reduced plate area subjected to a moving load system can be obtained as follows:

$$\mathbf{M}_A\ddot{\mathbf{q}}_A + \mathbf{C}_A\dot{\mathbf{q}}_A + \mathbf{K}_A\mathbf{q}_A = \mathbf{Q}_A + \mathbf{Q}_{flowA} \tag{30}$$

where $\mathbf{M}_A$, $\mathbf{C}_A$, $\mathbf{K}_A$, $\mathbf{Q}_A$, and $\mathbf{Q}_{flowA}$ are derived by assembling the MPEs, and $\mathbf{q}_A$ is the generalized coordinate vector that includes all the generalized coordinates of MPEs. Because the vibration of the plate at the boundary of the reduced plate area is close to zero, the boundary condition of the whole model is considered as clamped, which can be expressed as

$$w|_{BS} = 0, \left.\frac{\partial w}{\partial x}\right|_{BS} = \left.\frac{\partial w}{\partial y}\right|_{BS} = 0 \tag{31}$$

where *BS* is the boundary of the reduced plate area. These dynamic equations are solved numerically using the stiff differential equations solver ode15s [22] in MATLAB.

3 Validation

The accuracy of the MPE in solving basic plate structure subjected to moving load with arbitrary moving trajectories is verified here. Two different thin plate structures resting on Winkler ground and subjected to moving load cases are considered here, as shown in Fig. 2, where the load moves in four different trajectories including straight trajectories o_sB_1, o_sB_2, and o_sB_3, and curved trajectory o_sB_4. In these two cases, the length *a* and width *b* of the plate are both 80 m. The Young's modulus of plate *E* is 2.1×10^{11} N/m^2, the density of the plate ρ is 7850 kg/m^3, and Poisson's ratio ν is 0.3. The Winkler ground has an equivalent stiffness of 3.503×10^7 N/m and a damping of 1.7325×10^6 N·s/m. The thickness of the plate h in case 1 and case 2 is 0.05 m. In Fig. 2, $x_0=10$ m, $x_1=30$ m, $x_2=50$ m, $x_3=15$ m, $x_4=44.2$ m, $y_0=10$ m, $y_1=30$ m, $y_2=50$ m, $y_3=20$ m, $y_4=24.6$ m, and $z_0=0.5h$. The moving load has a constant value of 50000 N. When the load moves along trajectory o_sB_3, the load moving velocity $V_x(t)$ is 20 m/s, and the load moving velocity $V_y(t)$ is 20 m/s as the load moves along trajectory o_sB_1. When the load moves in trajectory o_sB_2, $V_x(t)$ and $V_y(t)$ are both 20 m/s. When the load moves in trajectory o_sB_4, the load linear velocity $V(t)=\left|\sqrt{V_x^2(t)+V_y^2(t)}\right|$ is 20 m/s. The dynamic responses of the plate were calculated using the MPE with 576 elements of 0.5 m length and width each, and the results were compared with those from semi analytical method developed in Ref. [19] and the commercial software ANSYS. In semi-analytical method, the first 500 modes are considered, and 640000 SHELL63

elements of 0.1 m length and width are used in ANSYS. All of the present MPE, semi-analytical method and ANSYS results converged. When considering the MPE, the shape of the reduced plate area is considered as a square with a side length of 12 m.

With different load moving trajectories considered, the time histories of the vertical displacement of the plate in different cases at different points are shown in Fig. 3 and Fig. 4, and the maximum relative differences between these results from the MPE and ANSYS SHELL63 at different points are included in Table 1. As presented in Fig. 3, Fig. 4, and Table 1, with different plate parameters and load moving trajectories considered, the results from the MPE are in good agreement with those from the ANSYS SHELL63, and their maximum relative difference is no more than 1.30 %.

The convergence of the MPE is further shown here. Considering the converged ANSYS SHELL63 results of the time history of vertical displacement of point A_2, the maximum relative differences between the results from the MPE and ANSYS SHELL63 with different numbers of MPEs used in modeling are presented in Fig. 5. As shown in Fig. 5, when 72 elements are used in the modeling, the relative difference between the results from the MPE and ANSYS SHELL63 is reduced to 0.5 %, and it is further reduced to 0.37 % when 90 elements are used in the modeling. With more than 90 elements used, the relative difference converged at 0.37 %. Based on this, the MPE shows good convergence in the calculation, and its accuracy is further verified here.

The MPE is then verified with different boundary conditions. While the clamped boundary condition has been applied in the above calculation, the simply supported boundary condition

Journal of Vibration and Acoustics. Received August 20, 2021;
Accepted manuscript posted December 27, 2021. doi:10.1115/1.4053474

is further considered here in the calculation of the dynamic responses of point A_1 with MPE, and the results are compared with those of the clamped condition and the ANSYS. It can be seen from Fig. 6 that with different boundary condition considered, there are some difference between different calculation results, but the difference is small and the simply supported boundary condition can also provide accurate results compared to those from the ANSYS. The maximum relative difference between the results from the simply supported and ANSYS is no more than 2.8 %. With enough length of the reduced plate area, different boundary condition can have familiar calculation results from the MPE.

The vertical displacement field of a plate subjected to a moving load is further considered here to verify the basic theory of the MPE. The vertical displacement contour maps of the plate in case 2 at different times when the load moves along trajectory $o_s B_4$ are shown in Fig. 7. As depicted in Fig. 7, when the load moves at the plate, the vibration of the plate mainly concentrates on a rectangular area around the moving load. Moreover, with the load moving along the trajectory, the plate vertical displacement field shows that the vibration of the plate follows the moving load, and the corresponding rectangular area remains the same. The length of this rectangular area is 7.82 m, which is smaller than the length of the truncated plate area. This phenomenon shows that the vibration of the plate far from the moving load is obviously attenuated to zero owing to the damping effect, which verifies the basic theory of the MPE.

4 Application of the MPE on vehicle–pavement interaction dynamic analysis

After the validation and investigation of the MPE, a vehicle-pavement interaction case is chosen here to further present the application of MPE in vehicle–pavement interaction dynamic

analysis in both constant and variable speed. A 7-DOF vehicle [9] interaction with road pavement is considered here, where the road is modeled as a single layer, rectangular thin plate on a viscoelastic foundation [17], as shown in Fig. 8.

The vehicle model considered here consist of a car body and four tires. The car body is supported on four tires through the vehicle suspension. The car body and tire are treated as rigid bodies, and the vertical, roll, and pitch motions of the car body and the vertical motion of tires are taken into account. The motions of the car body are described by z_v, θ_{xv}, and θ_{yv} and that of tire *i* is described by z_{ti} .The vehicle suspension is treated as a spring–damper element, where the stiffness and damping of the front suspension are described by K_{s1} and C_{s1}, and the stiffness and damping of the rear suspension are described by K_{s2} and C_{s2}, respectively. Using the multibody dynamic method, the vehicle model of seven degrees of freedom (DOFs) is established. The dynamic equations of the vehicle are

$$\mathbf{M}_v\ddot{\mathbf{q}}_v + \mathbf{C}_v\dot{\mathbf{q}}_v + \mathbf{K}_v\mathbf{q}_v = \mathbf{Q}_v \tag{32}$$

where

$$\mathbf{M}_v = diag\begin{bmatrix} m_v & I_{cx} & I_{cy} & m_{t1} & m_{t2} & m_{t3} & m_{t4} \end{bmatrix} \tag{33}$$

$$\mathbf{C}_v = \begin{bmatrix} \mathbf{C}_{11} & \mathbf{C}_{12} \\ symm. & \mathbf{C}_{22} \end{bmatrix}, \mathbf{K}_v = \begin{bmatrix} \mathbf{K}_{11} & \mathbf{K}_{12} \\ symm. & \mathbf{K}_{22} \end{bmatrix} \tag{34}$$

$$\mathbf{Q}_v = \begin{bmatrix} m_v g & 0 & 0 & m_{t1}g - F_{Ty1} & m_{t2}g - F_{Ty2} & m_{t3}g - F_{Ty3} & m_{t4}g - F_{Ty4} \end{bmatrix}^T \tag{35}$$

$$\mathbf{q}_v = \begin{bmatrix} z_v & \theta_{xv} & \theta_{yv} & z_{t1} & z_{t2} & z_{t3} & z_{t4} \end{bmatrix}^T \tag{36}$$

in which m_v is the mass of car body, I_{cx} and I_{cy} are the inertia moments of car body, and m_{ti} (i = 1, 2, 3, and 4) are the mass of tire *i*, respectively. *g* is the gravitational acceleration, and F_{Tyi} (i = 1, 2, 3, and 4) are the tire-pavement vertical interaction forces of tire *i*, respectively. In Eq. (34), there are

Journal of Vibration and Acoustics. Received August 20, 2021;
Accepted manuscript posted December 27, 2021. doi:10.1115/1.4053474

$$\mathbf{C}_{11}=\begin{bmatrix} 2\left(C_{s1}+C_{s2}\right) & 0 & 2\left(C_{s1}l_{x1}-C_{s2}l_{x2}\right) \\ & 2\left(C_{s1}l_y^2+C_{s2}l_y^2\right) & \\ \textit{symm.} & & 2\left(C_{s1}l_{x1}^2+C_{s2}l_{x2}^2\right) \end{bmatrix} \tag{37}$$

$$\mathbf{C}_{12}=\begin{bmatrix} -C_{s1} & -C_{s2} & -C_{s1} & -C_{s2} \\ -C_{s1}l_y & -C_{s2}l_y & C_{s1}l_y & C_{s2}l_y \\ -C_{s1}l_{x1} & C_{s2}l_{x2} & -C_{s1}l_{x1} & C_{s2}l_{x2} \end{bmatrix} \tag{38}$$

$$\mathbf{C}_{22}=diag\left[C_{s1}\quad C_{s2}\quad C_{s1}\quad C_{s2}\right],\ \mathbf{K}_{22}=diag\left[K_{s1}\quad K_{s2}\quad K_{s1}\quad K_{s2}\right] \tag{39}$$

$$\mathbf{K}_{11}=\begin{bmatrix} 2\left(K_{s1}+K_{s2}\right) & 0 & 2\left(K_{s1}l_{x1}-K_{s2}l_{x2}\right) \\ & 2\left(K_{s1}l_y^2+K_{s2}l_y^2\right) & \\ \textit{symm.} & & 2\left(K_{s1}l_{x1}^2+K_{s2}l_{x2}^2\right) \end{bmatrix} \tag{40}$$

$$\mathbf{K}_{12}=\begin{bmatrix} -K_{s1} & -K_{s2} & -K_{s1} & -K_{s2} \\ -K_{s1}l_y & -K_{s2}l_y & K_{s1}l_y & K_{s2}l_y \\ -K_{s1}l_{x1} & K_{s2}l_{x2} & -K_{s1}l_{x1} & K_{s2}l_{x2} \end{bmatrix} \tag{41}$$

where l_{x1} and l_{x2} are the wheel spaces and l_y is the half of the wheel track.

The pavement and viscoelastic foundation are then modeled. After the modeling of single MPE, the pavement near the vehicle is reduced to a small region around the vehicle and meshed using the MPE. Based on the finite element assembly theory, the dynamic equations of the reduced pavement model are

$$\mathbf{M}_p\ddot{\mathbf{q}}_p+\mathbf{C}_p\dot{\mathbf{q}}_p+\mathbf{K}_p\mathbf{q}_p=\mathbf{Q}_{pF}+\mathbf{Q}_{pG}+\mathbf{Q}_{pflow} \tag{42}$$

where $\mathbf{M}_p$, $\mathbf{C}_p$, and $\mathbf{K}_p$ are the mass, damping and stiffness matrices of the reduced pavement model, respectively, $\mathbf{Q}_{pflow}$ is the additional generalized force vector and it is close to zero, $\mathbf{q}_p$ is the generalized coordinate vector of the reduced pavement model, $\mathbf{Q}_{pF}$ is the generalized force vector caused by F_{Tyi}, and $\mathbf{Q}_{pG}$ is the generalized force vector caused by the reaction force of the foundation.

The generalized force vector $\mathbf{Q}_{pG}$ is derived as follows. By considering an arbitrary

point on the pavement and its vertical displacement and velocity are z_p and $\dot{z}_p$, the corresponding foundation reaction force can be expressed as

$$F_g = K_g z_p + \beta_g K_g z_p^2 + C_g \dot{z}_p \tag{43}$$

where K_g and C_g are the equivalent stiffness and damping of the foundation, respectively, and β_g is the cubic nonlinear coefficient. Based on the virtual work principle [21], the generalized force vector caused by the foundation reaction force of one single MPE is

$$\mathbf{Q}_{pGM} = \iint_S \left(\mathbf{N}^T \begin{pmatrix} -K_g \mathbf{N}\mathbf{q} + C_g \begin{pmatrix} V_x(t)\mathbf{N}_x \\ +V_y(t)\mathbf{N}_y \end{pmatrix} \mathbf{q} \\ -C_g \mathbf{N}\dot{\mathbf{q}} - \beta K_g (\mathbf{N}\mathbf{q})^2 \end{pmatrix} \right) dxdy \tag{44}$$

where S is the area of the single MPE and $\mathbf{N}$ is the shape function vector of MPE. In Eq. (44), there are $\mathbf{N}_x = \frac{\partial \mathbf{N}}{\partial x}$ and $\mathbf{N}_y = \frac{\partial \mathbf{N}}{\partial y}$. Eq. (44) is solved using the Gaussian quadrature method. Based on $\mathbf{Q}_{pGM}$, $\mathbf{Q}_{pG}$ can be derived through using the finite element assembly theory.

The tire-pavement interaction forces are finally calculated. The expression of the tire-pavement interaction force of tire i is [9]

$$F_{Tyi} = K\left(z_{ti} - r_{si} - z_{pi}\right) + \beta K\left(z_{ti} - r_{si} - z_{pi}\right)^2 + C\left(\dot{z}_{ti} - \dot{r}_{si} - \dot{z}_{pi}\right) \tag{45}$$

where r_{si} is the road surface roughness and z_{pi} is the pavement vertical displacement at the tire i tire-pavement contact point. K is the linear tire stiffness, β is the nonlinear tire stiffness coefficient, and C is the tire damping coefficient. The r_{si} can be calculated using the following functions

$$r_1 = r_3 = A\sin\left(\frac{2\pi V t}{L_0}\right), r_2 = r_4 = A\sin\left(\frac{2\pi}{L_0}\left(Vt + l_{x1} + l_{x2}\right)\right) \tag{46}$$

where L_0 is the wavelength of harmonic road roughness. Note that z_{ti} and z_{pi} change at every time step due to F_{Tyi}; thus Eqs. (32) and (42) are coupled through tire-pavement

interaction forces.

Based on Eqs. (32) and (42), the governing equations of the vehicle-pavement interaction model are expressed as

$$\begin{bmatrix} \mathbf{M}_v & \\ & \mathbf{M}_p \end{bmatrix}\begin{bmatrix} \ddot{\mathbf{q}}_v \\ \ddot{\mathbf{q}}_p \end{bmatrix}+\begin{bmatrix} \mathbf{C}_v & \\ & \mathbf{C}_p \end{bmatrix}\begin{bmatrix} \dot{\mathbf{q}}_v \\ \dot{\mathbf{q}}_p \end{bmatrix}+\begin{bmatrix} \mathbf{K}_v & \\ & \mathbf{K}_p \end{bmatrix}\begin{bmatrix} \mathbf{q}_v \\ \mathbf{q}_p \end{bmatrix}=\begin{bmatrix} \mathbf{Q}_v \\ \mathbf{Q}_{pF}+\mathbf{Q}_{pG}+\mathbf{Q}_{pflow} \end{bmatrix} \tag{47}$$

The parameters of the vehicle–pavement interaction system are listed in Table 2.

Let the vehicle move along the pavement, as shown in Fig. 9. The length of road L is 400 m, and the width of the road H is 10 m. The vehicle starts at a position d_0 = 30 m. The vehicle running with constant speed 72 km/h and initial speed 36 km/h and acceleration 4 m/s^2 are both considered here. The dynamic responses of the vehicle–pavement interaction are solved using the MPE, where 1296 elements are used in meshing the reduced plate area with length of 36 m and width of 6 m. To further verify the accuracy of the MPE, the traditional model of the vehicle–pavement interaction is used here, where the full plate is modeled using Galerkin's method and 800 modes of the x direction and 20 modes of the y direction are considered in the modeling. The commercial software MATLAB was utilized to achieve these two models and the function ode15s was used to solve their dynamic equations. The calculation time of these two methods is 10 s, and their calculation steps are both 0.001 s. The initial condition of the generalized coordinate array was zero. Details of the traditional model can be found in Ref. [9].

The time histories of vertical displacement of the tire 1 and tire 2 with different vehicle velocity are shown in Fig. 10, and the time histories of vertical displacement of the plate at different points are shown in Fig. 11. As shown in Fig. 10, when the vehicle moves with constant speed, the vibration of the tire 1 and tire 1 keeps stable, and their maximum vertical displacement has little changes. But when the vehicle moves with variable speed, both the

Journal of Vibration and Acoustics. Received August 20, 2021;
Accepted manuscript posted December 27, 2021. doi:10.1115/1.4053474

vertical displacement of the tire 1 and tire 2 increases with the increasing of the speed. Moreover, the calculation results from the MPE are in very good agreement with those from the traditional method, and their maximum relative difference is no more than 0.78 %. Without loss of generality, one fixed point A and tire–pavement interaction point of tire 1 are selected to present the dynamic responses of the pavement, where $d_1 = 100$ m. It can be observed from Fig. 11 that the front tire load is much smaller than the rear one. When the vehicle passes the fixed point, the vertical displacement of point A caused by the front tire is 0.324 mm, and that caused by the rear tire is 0.698 mm. Also, with the increasing of the speed, the vertical displacement of the plate at tire 1 tire-pavement interaction point increases. In addition, the dynamic responses resulting from the MPE are in good agreement with those from the traditional method, and their maximum relative difference is no more than 0.75 %. The vertical displacement field of the pavement at different times is shown in Fig. 12. As shown in Fig. 12, the vibration of the plate concentrates on the adjacent area of the tire–pavement interaction point, while the vibration of the plate at other areas is almost zero. This further verifies the basic theory of the MPE.

The vehicle velocity and vehicle mass are the two main parameters of the road vehicle, and their influence on the plate dynamic responses in vehicle–pavement interaction dynamics are investigated using the MPE and traditional methods. The influence of vehicle velocity and vehicle mass on the maximum vertical displacement of the plate at point A are shown in Fig. 13. As depicted in Fig. 13, the maximum vertical displacement of the plate slowly increases with the increasing speed of the vehicle, but it increases obviously with increasing vehicle mass. Because the road vehicle velocity can barely exceed 160 km/h, especially for heavy vehicles, the pavement may not be damaged owing to high-speed vehicle–pavement interaction.

However, because the vibration of the pavement is obviously influenced by the vehicle mass, the pavement is easily damaged by an overweight vehicle. This phenomenon can also be observed in many roads with heavy vehicle traffic. In addition, the results from the MPE are in good agreement with those from the traditional model, and their maximum relative difference is no more than 0.75 %.

5. Efficiency of the MPE in vehicle-pavement dynamic analysis

While the accuracy of the MPE in solving vehicle-pavement interaction dynamic responses has been verified before, its efficiency compared to the traditional method is illustrated here. Because all of the above cases are achieved in MATLAB and solved using a computer with Windows 10 and a 4.00 GHz Inter i7-6700K processor with 32 GB RAM, the vehicle moving distance and its corresponding model length of the MPE and MSM, the DOFs of the vehicle–pavement models obtained by the traditional model using the MSM and present model using the MPE, and the calculation times of different models are listed in Table 3.

As can be observed in Table 3, when considering the plate structure, the reduction in DOFs of the plate structure by using the MPE compared to the traditional method is much more obvious because the plate structure should consider both the x and y directions. When considering the vehicle–pavement interaction, the DOFs of the MPE model are only one-tenth of those of the traditional MSM model, and the CPU time usage of the MPE is approximately one-third of that of the traditional MSM model. Note that the calculation results of the MSM and MPE model should have a similar accuracy before comparing their efficiency, and the number of modes used in the MSM should be adjusted according to the length of the MSM model to ensure its calculation accuracy. This has caused the large number of modes used in

the MSM model with the 350 m vehicle moving distance considered. It should be further mentioned that if the road surface roughness is not considered in the vehicle–pavement interaction, the CPU time usage of the MPE can be further reduced to 587 s, which is almost one-tenth of that of the MSM. Based on these results, the MPE has remarkable advantages in solving problems of complex plate structures subjected to moving loads.

6 Conclusions

A new MPE based on the Kirchhoff–Love theory and ALE formulation is developed to efficiently and accurately calculate the dynamic responses of vehicle-pavement interaction. The wide plate structure is reduced to a small rectangular plate area around the moving load, and then this reduced plate area is included in a moving control volume attached to the moving load and described in the corresponding relative coordinate system. The ALE formulation is first considered here to describe the relative motion between the plate material point and the MPE, and the Lagrange's equation is finally used to obtain its final dynamic equations. Because only the small reduced plate area needs to be modeled, the efficiency of the MPE is significantly increased compared to the traditional FEM and MSM in calculating the dynamic responses of a wide plate structure under a moving load. In addition, because the ALE formulation is considered here, the MPE can calculate the dynamic responses of the plate structure under loads moving along an arbitrary trajectory in the long term. The MPE is a valuable tool in the investigation of problems of vehicle-pavement interaction dynamic behavior in a long-term.

After the validation of the present MPE with two simple plate subjected to moving load cases with different load moving trajectories, the influence of different factors on reduced plate area length of the RBM model is analyzed here to help researchers better understand the MPE,

and it is then applied in the analysis of the vehicle–pavement interaction dynamics with constant and variable speed. The investigation results show that the MPE is accurate and efficient in solving vehicle–pavement interaction with only one-tenth of the DOFs and one-third of the calculation times required by the traditional model with the MSM. In addition, it was found that the load moving velocity and ground damping have a significant influence on plate vibration propagation, where high load moving velocity and low ground damping cause long reduced plate area length. Based on the calculation results of the vehicle–pavement interaction dynamics using the present MPE model and traditional model, the vehicle load is the main factor affecting the pavement dynamic responses compared to its velocity.

Based on the present MPE, an efficient way to decide the side length of the reduced plate area in different vehicle-pavement interaction cases will be developed, and the dynamic characteristics of the vehicle-pavement interaction with more complex road and vehicle factors and vehicle moves along curved trajectory on the road will be investigated in the future. This will further strengthen the theory and application value of the MPE.

Acknowledgements

This work was supported by the National Natural Science Foundation of China (grant numbers 12072293, 11772100, and 11802188) and Project of the State Key Laboratory of Traction Power, Southwest Jiaotong University (grant number 2021TPL-T10).

References

[1] Grakovski, A., and Pilipovecs, A., 2017, “Dynamics of Interaction between the Road

Surface and Vehicle's Wheel in Fibre-Optic System for Automatic Weighing in Motion of Transport," Procedia Engineering, **178**, pp. 5–12.

[2] Romero, J. A., Lozano-Guzmán, A. A., Obregón-Biosca, S. A., and Betanzo-Quezada, E., 2018, "A Plane Model of the Interaction of a Vehicle with the Road Infrastructure," Advances in Engineering Software, **117**, pp. 46–58.

[3] Kim, R. E., 2020, "Classification of Variable Foundation Properties Based on Vehicle–Pavement–Foundation Interaction Dynamics," Sensors (Switzerland), **20**(21), pp. 1–17.

[4] Ding, H., Yang, Y., Chen, L. Q., and Yang, S. P., 2014, "Vibration of Vehicle-Pavement Coupled System Based on a Timoshenko Beam on a Nonlinear Foundation," Journal of Sound and Vibration, **333**(24), pp. 6623–6636.

[5] Patil, V. A., Sawant, V. A., and Deb, K., 2013, "2-D Finite Element Analysis of Rigid Pavement Considering Dynamic Vehicle-Pavement Interaction Effects," Applied Mathematical Modelling, **37**(3), pp. 1282–1294.

[6] Xu, X., Akbarian, M., Gregory, J., and Kirchain, R., 2019, "Role of the Use Phase and Pavement-Vehicle Interaction in Comparative Pavement Life Cycle Assessment as a Function of Context," Journal of Cleaner Production, **230**, pp. 1156–1164.

[7] Wang, H., Al-Qadi, I. L., and Stanciulescu, I., 2012, "Simulation of Tyre-Pavement Interaction for Predicting Contact Stresses at Static and Various Rolling Conditions," International Journal of Pavement Engineering, **13**(4), pp. 310–321.

[8] Ling, D. sheng, Zhao, Y., Huang, B., Zhang, F., and Zhou, Y., 2018, "Analysis of Dynamic Stress Path in Inhomogenous Subgrade under Moving Aircraft Load," Soil

Dynamics and Earthquake Engineering, **111**(April), pp. 65–76.

[9] Li, S., Yang, S., and Chen, L., 2013, "A Nonlinear Vehicle-Road Coupled Model for Dynamics Research," Journal of Computational and Nonlinear Dynamics, **8**(2), pp. 1–14.

[10] Behnke, R., Wollny, I., Hartung, F., and Kaliske, M., 2019, "Thermo-Mechanical Finite Element Prediction of the Structural Long-Term Response of Asphalt Pavements Subjected to Periodic Traffic Load: Tire-Pavement Interaction and Rutting," Computers & Structures, **218**, pp. 9–31.

[11] Shi, X. M., and Cai, C. S., 2009, "Simulation of Dynamic Effects of Vehicles on Pavement Using a 3D Interaction Model," Journal of Transportation Engineering, **135**(10), pp. 736–744.

[12] Li, Q., Liu, J. Q., and Liu, H., 2015, "Random Dynamic Response Analysis of Asphalt Pavement Based on the Vehicle-Pavement Interaction," Applied Mechanics and Materials, **744**–**746**, pp. 1288–1297.

[13] Kim, S. M., Jose M. R., and Kenneth. H. S., 1999, "Numerical Simulation of Rolling Dynamic Deflectometer Tests," Journal of Transportation Engineering, **125**(2), pp. 85–92.

[14] Koh, C. G., Ong, J. S. Y., Chua, D. K. H., and Feng, J., 2003, "Moving Element Method for Train-Track Dynamics," International Journal for Numerical Methods in Engineering, **56**(11), pp. 1549–1567.

[15] Xu, W. T., Lin, J. H., Zhang, Y. H., Kennedy, D., and Williams, F. W., 2009, "2D Moving Element Method for Random Vibration Analysis of Vehicles on

Kirchhoffplate with Kelvin Foundation," Latin American Journal of Solids and Structures, **6**(January), pp. 169–183.

[16] Reddy, J. N., Nguyen, X. V., Than Cao, T. N., Lieu, Q. X., and Luong, V. H., 2020, "An Integrated Moving Element Method (IMEM) for Hydroelastic Analysis of Infinite Floating Kirchhoff-Love Plates under Moving Loads in a Shallow Water Environment," Thin-Walled Structures, **155**(July), p. 106934.

[17] Kim, R. E., Kang, S., Spencer, B. F., Al-Qadi, I. L., and Ozer, H., 2019, "Impact of Pavement Roughness and Deflection on Fuel Consumption Using Energy Dissipation," Journal of Engineering Mechanics, **145**(10), p. 04019080.

[18] Yang, C. J., Xu, Y., Zhu, W. D., Fan, W., Zhang, W. H., and Mei, G. M., 2020, "A Three-Dimensional Modal Theory-Based Timoshenko Fi Nite Length Beam Model for Train-Track Dynamic Analysis," Journal of Sound and Vibration, **479**, pp. 1–22.

[19] Bajer, C. I., and Dyniewicz, B., 2012, Numerical Analysis of Vibrations of Structures under Moving Inertial Load. Springer, New York.

[20] Hong, D., Tang, J., and Ren, G., 2011, "Dynamic Modeling of Mass-Flowing Linear Medium with Large Amplitude Displacement and Rotation," Journal of Fluids and Structures, **27**(8), pp. 1137–1148.

[21] Xu, Y., Zhu, W., Fan, W., Caijin, Y., and Zhang, W., 2019, "A New Three-Dimensional Moving Timoshenko Beam Element for Moving Load Problem Analysis," Journal of Vibration and Acoustics, **142**(June), pp. 1–39.

[22] Celaya, E. A., Aguirrezabala, J. J. A., and Chatzipantelidis, P., 2014, "Implementation of an Adaptive BDF2 Formula and Comparison with the MATLAB Ode15s," Procedia

Computer Science, **29**, pp. 1014–1026.

Journal of Vibration and Acoustics. Received August 20, 2021;
Accepted manuscript posted December 27, 2021. doi:10.1115/1.4053474

Table Captions List

Figure Captions List

Journal of Vibration and Acoustics. Received August 20, 2021;
Accepted manuscript posted December 27, 2021. doi:10.1115/1.4053474

tire-pavement interaction point with constant speed and (d) tire 1 tire-pavement interaction point with variable speed

Fig. 12 Vertical displacement field of the pavement at different time

Fig. 13 Influence of vehicle velocity and vehicle mass on pavement maximum vertical displacement at point *A*: (a) influence of vehicle velocity and (b) influence of vehicle mass

Journal of Vibration and Acoustics. Received August 20, 2021;
Accepted manuscript posted December 27, 2021. doi:10.1115/1.4053474

Table 1

Point	Maximum relative difference	Point	Maximum relative difference
A_1	1.21 %	B_1	1.20 %
A_2	0.37 %	B_2	0.40 %
A_3	1.30 %	B_3	1.21 %
A_4	1.18 %	A_5	1.05 %

Journal of Vibration and Acoustics. Received August 20, 2021;
Accepted manuscript posted December 27, 2021. doi:10.1115/1.4053474

Table 2

Notation	Item	Value	Unit
m_c	Mass of car body	1.5×10^4	kg
I_{cx}	Moment of inertia of car body about x-axis	3.0×10^5	kg · m^2
I_{cy}	Moment of inertia of car body about y-axis	0.6×10^5	kg · m^2
m_{tf}	Mass of front tire	190	kg
m_{tr}	Mass of rear tire	380	kg
K_{s1}	Vertical stiffness of front suspension system	3.7×10^5	N / m
C_{s1}	Vertical damping of front suspension system	12000	N · s / m
K_{s2}	Vertical stiffness of rear suspension system	9.2×10^5	N / m
C_{s2}	Vertical damping of rear suspension system	30000	N · s / m
l_{x1}	Longitudinal distance between front tire and center of car body	3.29	m
l_{x2}	Longitudinal distance between rear tire and center of car body	1.48	m
E	Young's modulus of the plate	2.4×10^{10}	N / m^2
ρ	Density of the plate	2613	kg / m^3
v	Poisson's ration of the plate	0.35	-
K_f	Front linear tire stiffness	0.73×10^6	N / m
C_f	Front tire damping coefficient	600	N · s / m
K_r	Rear linear tire stiffness	1.46×10^6	N / m
C_r	Rear tire damping coefficient	900	N · s / m
β	Nonlinear tire stiffness coefficient	0.01	-
K_g	Ground equivalent stiffness	4.8×10^7	N / m
C_g	Ground equivalent damping	0.3×10^6	N · s / m
β_g	Nonlinear ground stiffness coefficient	0.1	-
A	Amplitude of road surface roughness	0.002	m
L_0	Wavelength of harmonic road roughness	2.3	m

Journal of Vibration and Acoustics. Received August 20, 2021;
Accepted manuscript posted December 27, 2021. doi:10.1115/1.4053474

Table 3

Vehicle moving distance (m)	Length of the model		DOFs		CPU time (s)	
	MPE	MSM	MPE	MSM	MPE	MSM
350	36	400	1450	16007	28862	67299

Journal of Vibration and Acoustics. Received August 20, 2021;
Accepted manuscript posted December 27, 2021. doi:10.1115/1.4053474

Figure 1

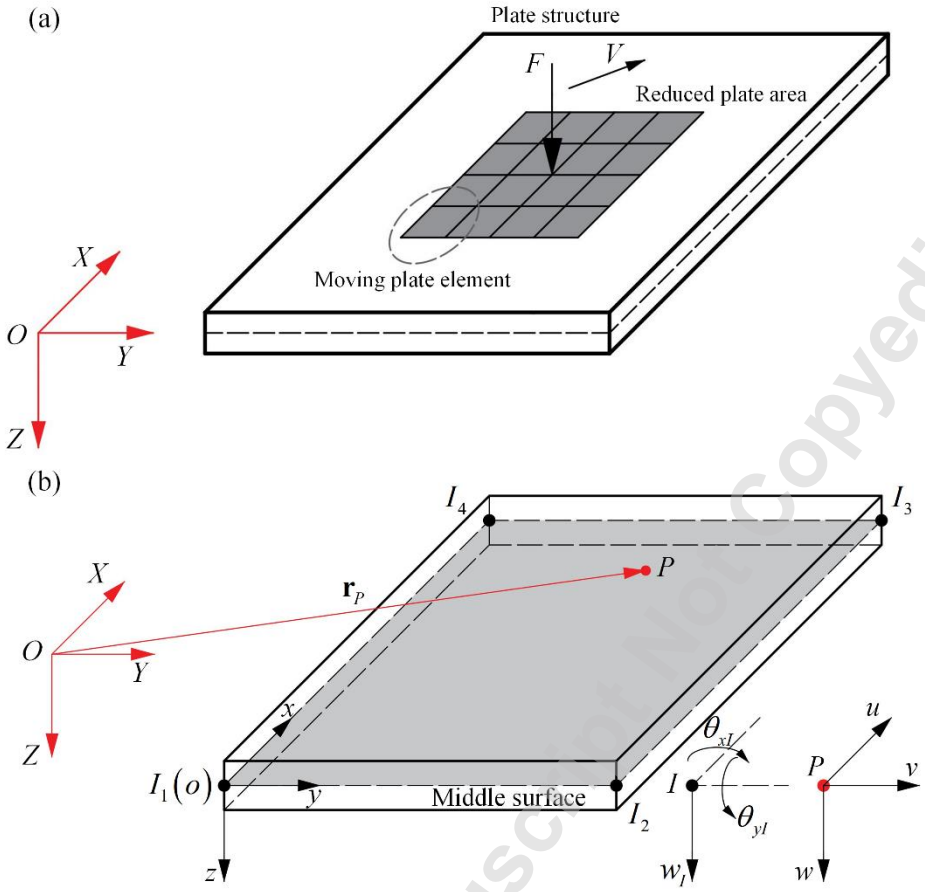

Journal of Vibration and Acoustics. Received August 20, 2021;
Accepted manuscript posted December 27, 2021. doi:10.1115/1.4053474

Figure 2

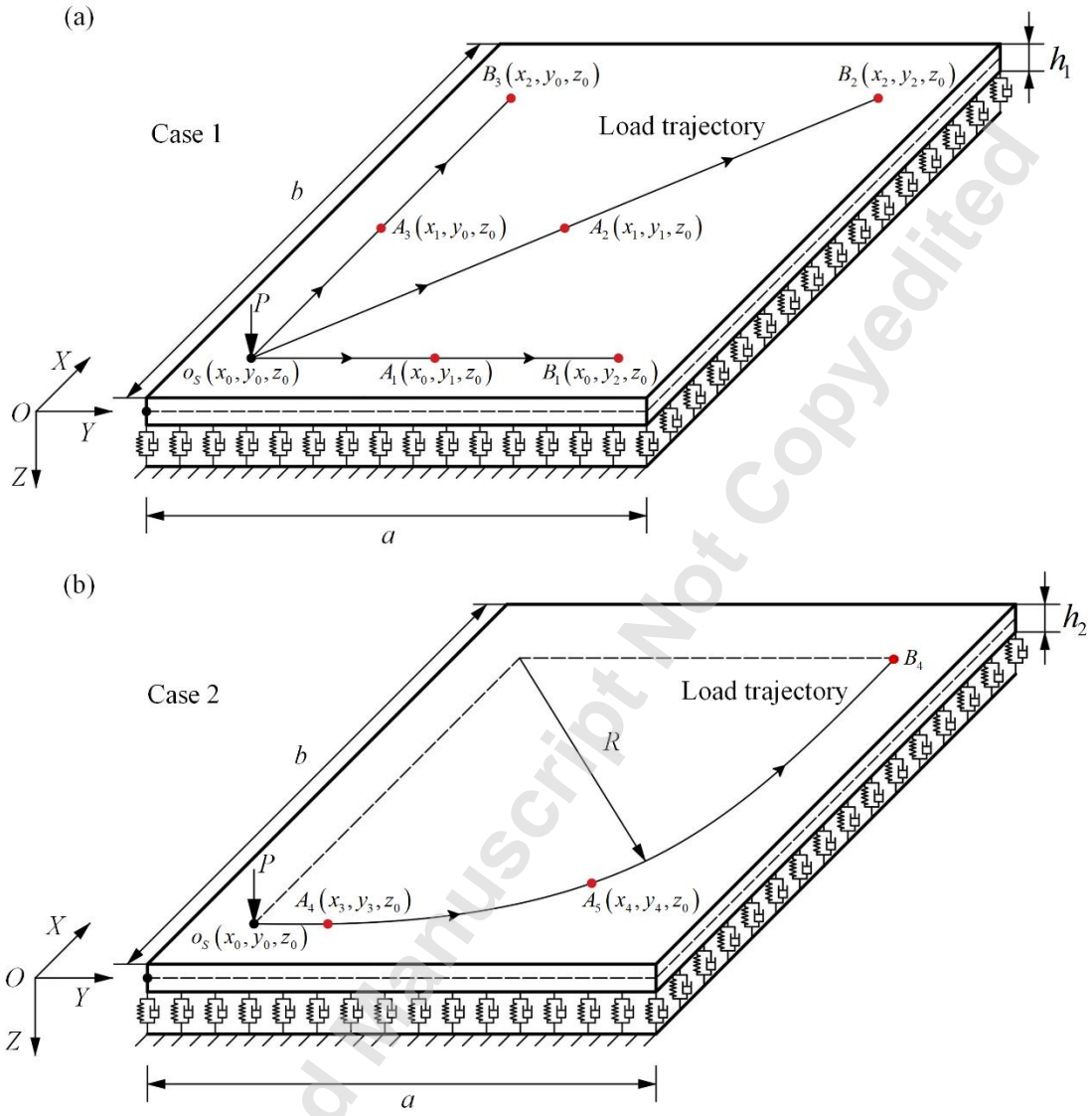

Journal of Vibration and Acoustics. Received August 20, 2021;
Accepted manuscript posted December 27, 2021. doi:10.1115/1.4053474

Figure 3

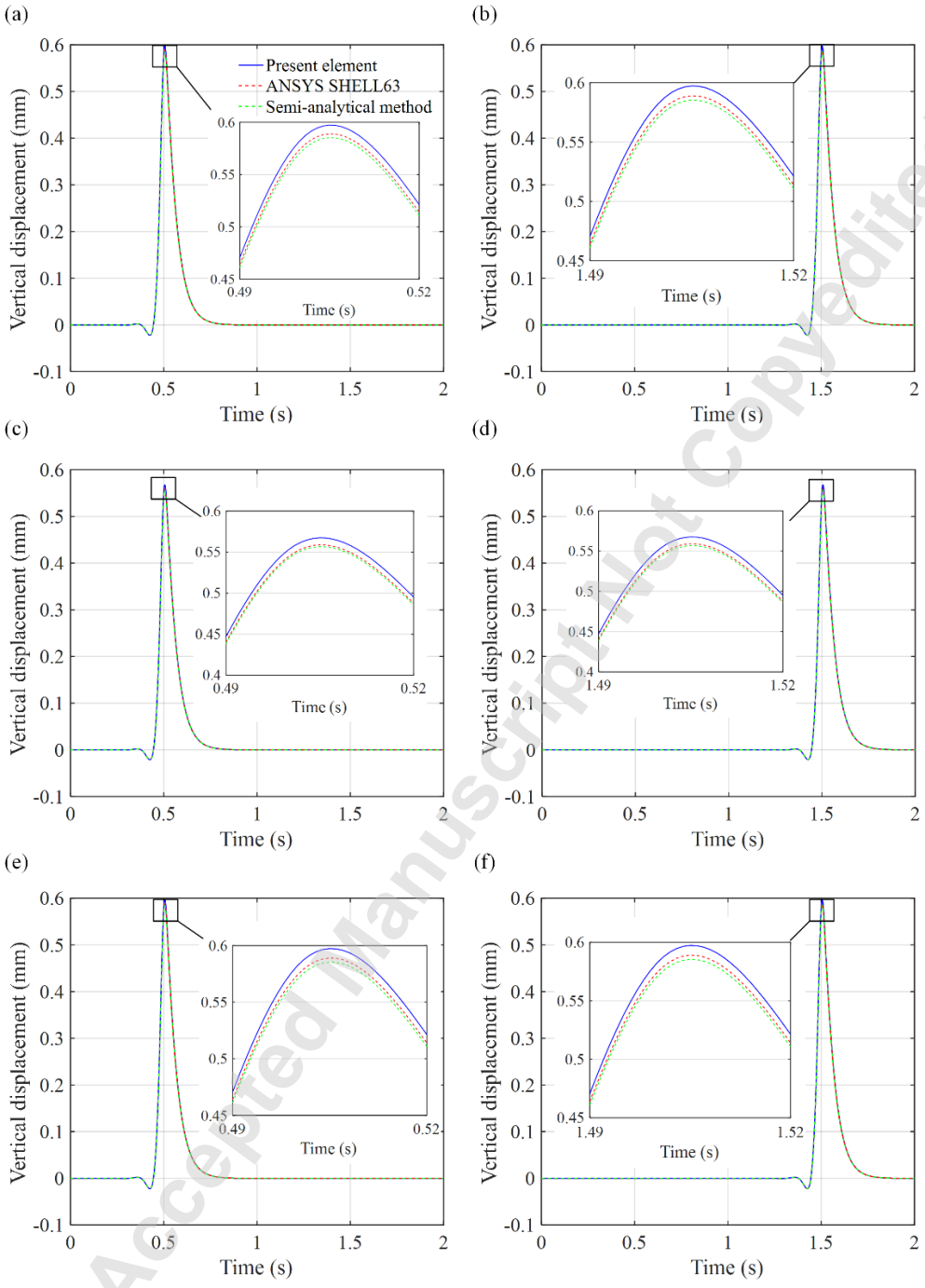

Journal of Vibration and Acoustics. Received August 20, 2021;
Accepted manuscript posted December 27, 2021. doi:10.1115/1.4053474

Figure 4

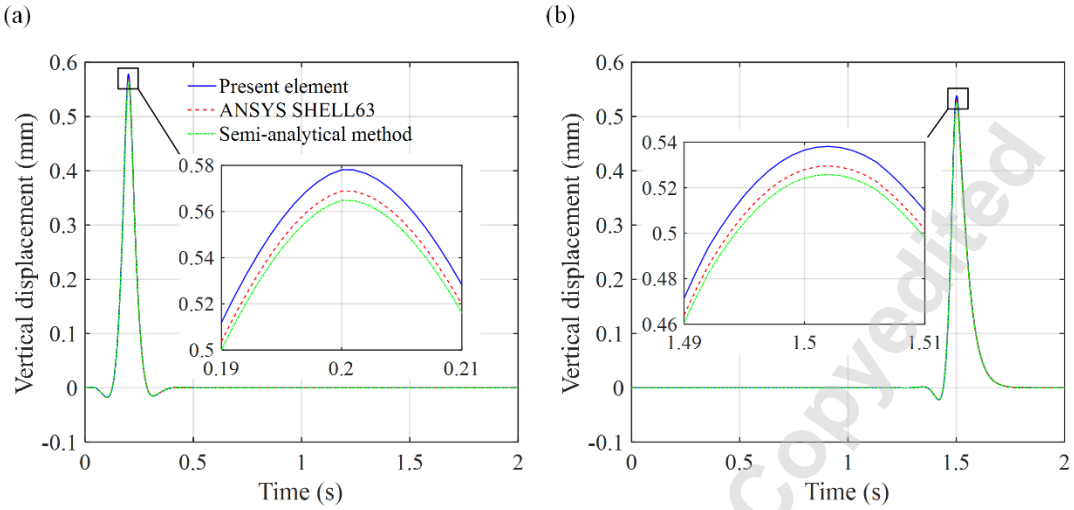

Journal of Vibration and Acoustics. Received August 20, 2021;
Accepted manuscript posted December 27, 2021. doi:10.1115/1.4053474

Figure 5

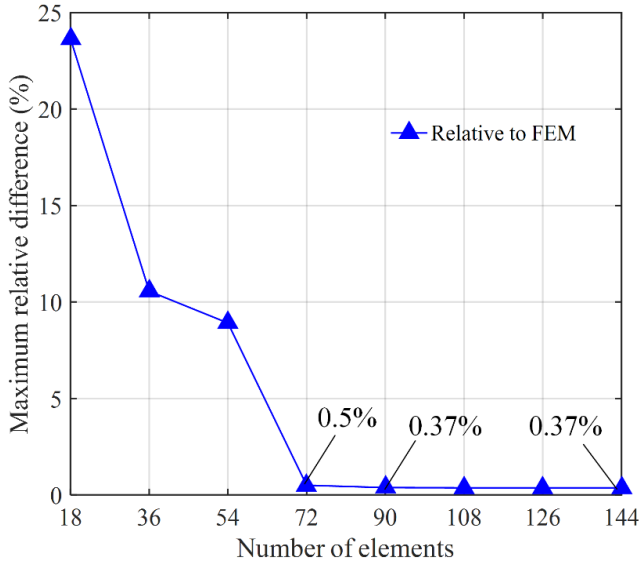

Journal of Vibration and Acoustics. Received August 20, 2021;
Accepted manuscript posted December 27, 2021. doi:10.1115/1.4053474

Figure 6

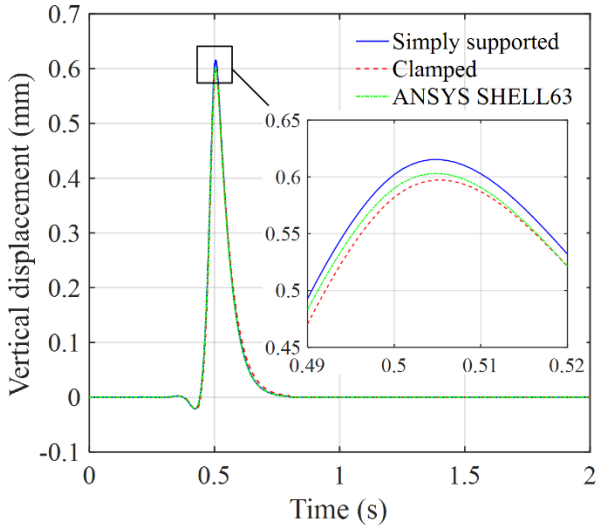

Journal of Vibration and Acoustics. Received August 20, 2021;
Accepted manuscript posted December 27, 2021. doi:10.1115/1.4053474

Figure 7

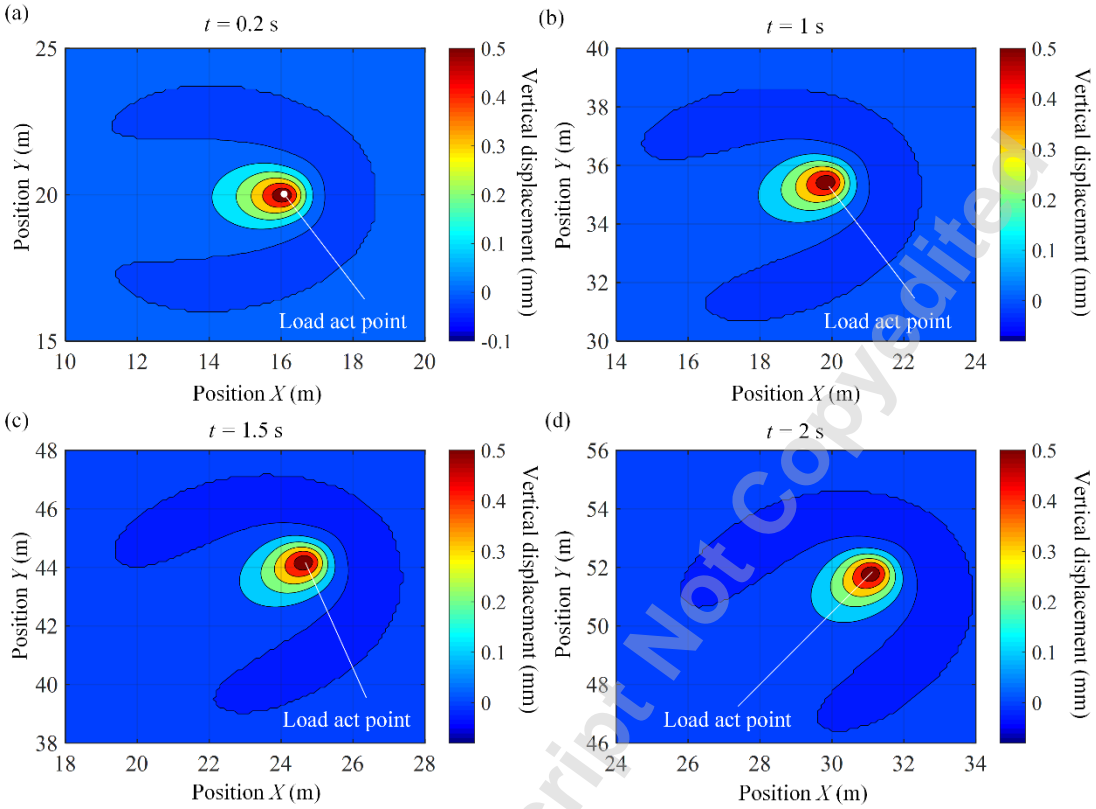

Journal of Vibration and Acoustics. Received August 20, 2021;
Accepted manuscript posted December 27, 2021. doi:10.1115/1.4053474

Figure 8

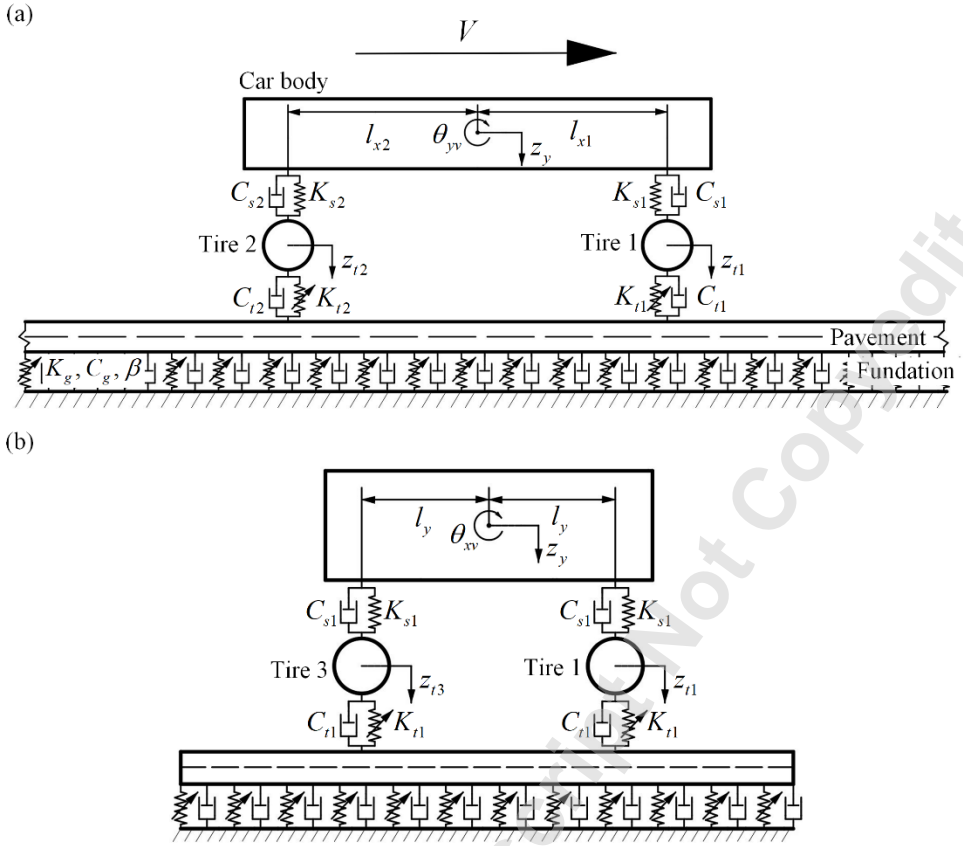

Journal of Vibration and Acoustics. Received August 20, 2021;
Accepted manuscript posted December 27, 2021. doi:10.1115/1.4053474

Figure 9

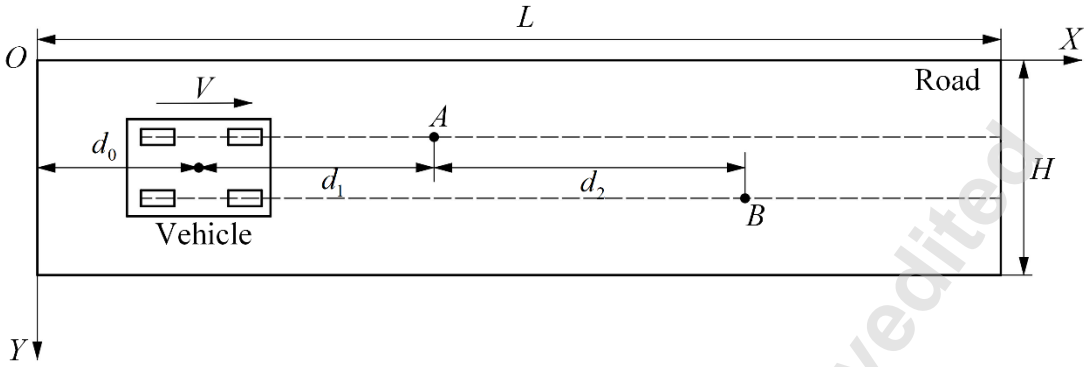

Journal of Vibration and Acoustics. Received August 20, 2021;
Accepted manuscript posted December 27, 2021. doi:10.1115/1.4053474

Figure 10

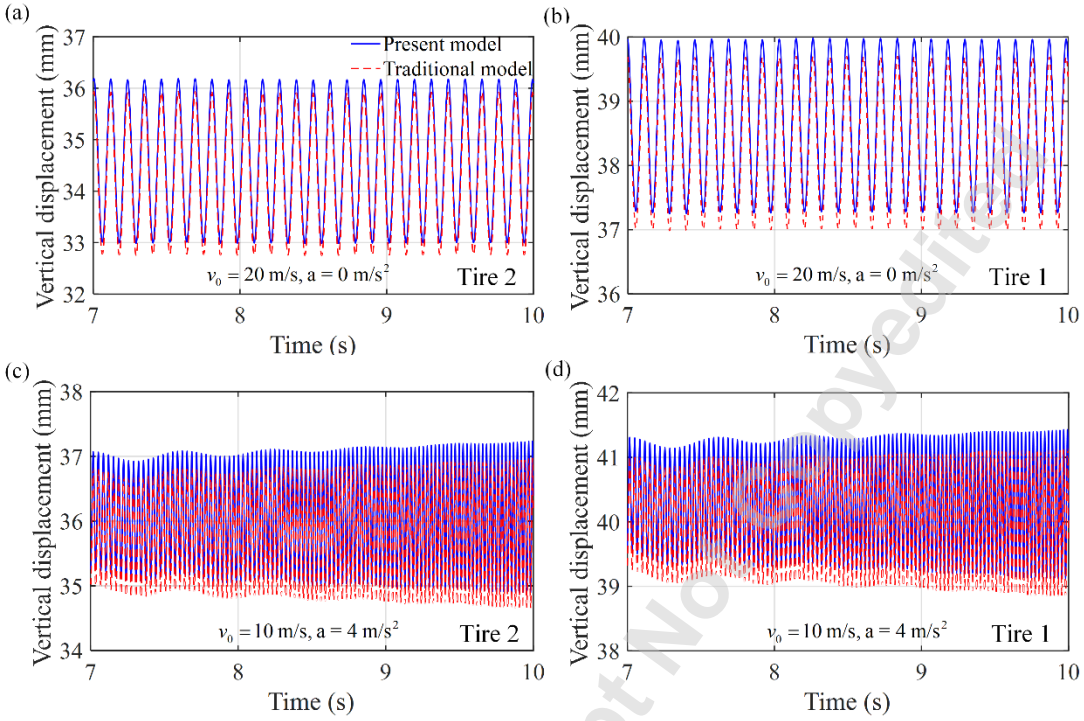

Journal of Vibration and Acoustics. Received August 20, 2021;
Accepted manuscript posted December 27, 2021. doi:10.1115/1.4053474

Figure 11

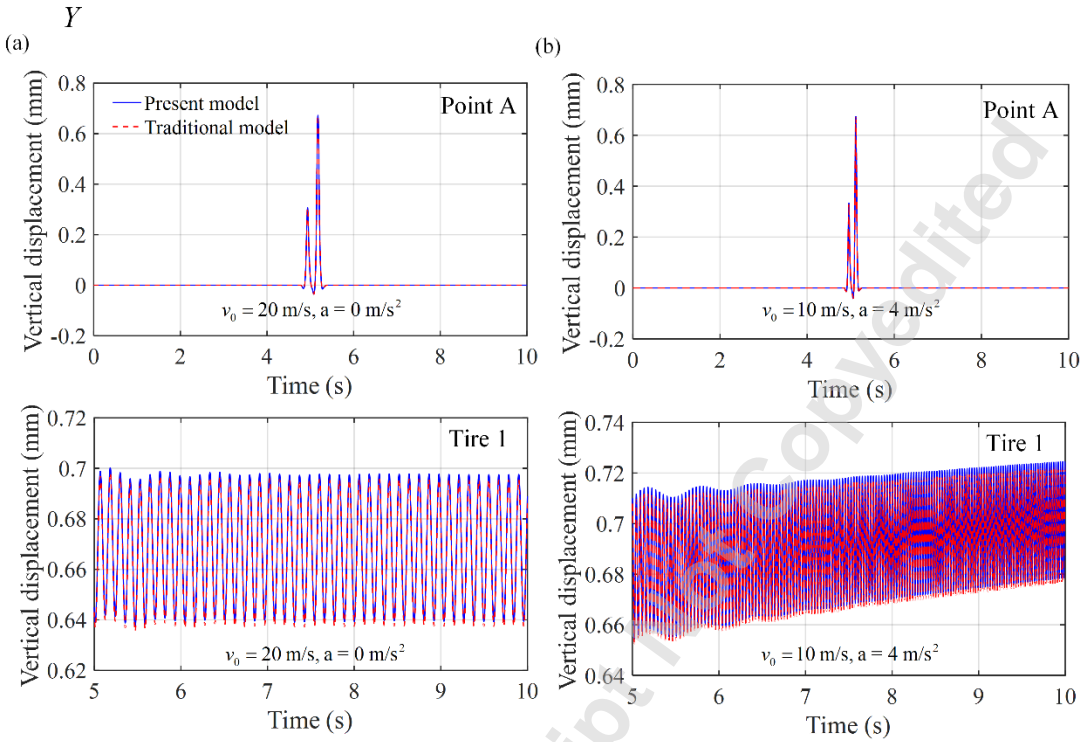

Journal of Vibration and Acoustics. Received August 20, 2021;
Accepted manuscript posted December 27, 2021. doi:10.1115/1.4053474

Figure 12

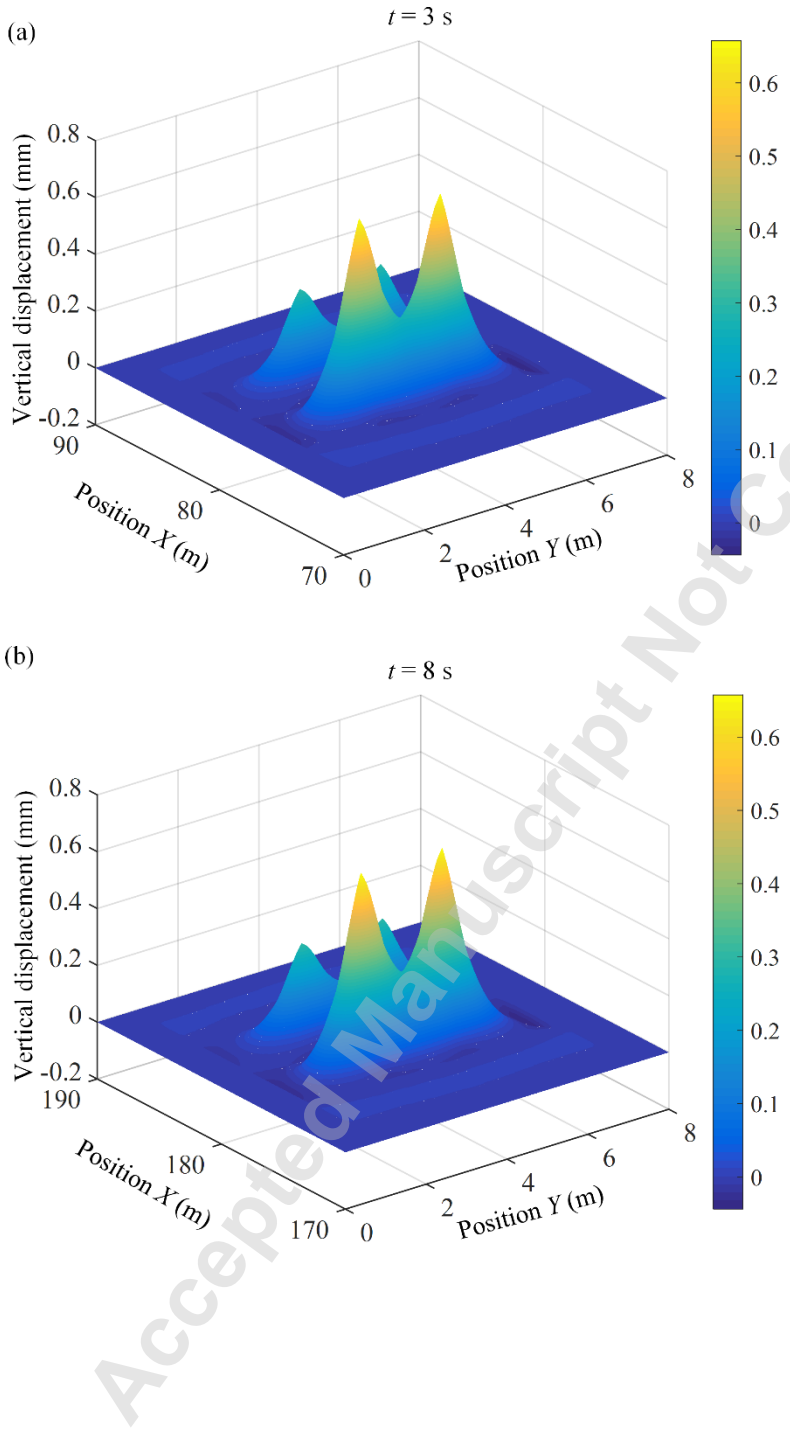

Journal of Vibration and Acoustics. Received August 20, 2021;
Accepted manuscript posted December 27, 2021. doi:10.1115/1.4053474

Figure 13